2015-12-01

Silicon Carbon Nanotube Lithium Ion Batteries

Lawrence Kent Barrett
Brigham Young University

Silicon Carbon Nanotube Lithium Ion Batteries

Lawrence Kent Barrett

A thesis submitted to the faculty of
Brigham Young University
in partial fulfillment of the requirements for the degree of

Master of Science

Robert C. Davis, Chair
Richard R. Vanfleet
David A. Allred

Department of Physics and Astronomy

Brigham Young University

December 2015

ABSTRACT

Silicon Carbon Nanotube Lithium Ion Batteries

Lawrence Kent Barrett
Department of Physics and Astronomy, BYU
Master of Science

Silicon has the highest theoretical capacity of any known anode material, and silicon coated carbon nanotubes (Si-CNTs) have shown promise of dramatically increasing battery capacity. However, capacity fading with cycling and low rate capability prevent widespread use. Here, three studies on differing aspects of these batteries are presented. Here, three studies on differing aspects of these batteries are presented. The first examines the rate capability of these batteries. It compares the cycling of electrodes hundreds of microns thick with and without ten micron access holes to facilitate diffusion. The holes do not improve rate capability, but thinner coatings of silicon do improve rate capability, indicating that the limiting mechanism is the diffusion through the nanoscale bulk silicon. The second attempts to enable stable cycling of anodes heavily loaded with silicon, using a novel monolithic scaffolding formed by coating vertically aligned carbon nanotubes (VACNTs) with nanocrystalline carbon. The structure was only able to stabilize the cycling at loadings of carbon greater than 60% of the electrode by volume. These electrodes have volume capacities of ~1000 mAhr/ml and retained over 725 mAhr/ml by cycle 100. The third studies the use of an encapsulation method to stabilize the solid electrolyte interphase (SEI) and exclude the electrolyte. The method was only able to stabilize cycling at loadings below 5% silicon, but exhibits specific capacities as high as 3000 mAhr/g of silicon after 20 cycles.

Keywords: silicon, lithium ion batteries, carbon nanotubes

ACKNOWLEDGMENTS

I would like to thank first and foremost my wife Erika, who has been infinitely understanding and supportive during this process.

I think part of what makes BYU special is the attention professors are willing to give students, even undergraduates. I have capitalized on this significantly over the last 5 years. Particular thanks is due to Drs. Allred, Davis, Vanfleet, and Harb for their understanding and support.

In addition, thanks are due to all of the students who have helped on this project over the years, including Kevin Laughlin, Rita Fan, Sterling Baird, Caleb Reidhead, Kenny Hinton, and Adam Stevens. Thanks guys.

TABLE OF CONTENTS

LIST OF FIGURES

Chapter 1

Introduction

Much has been written about filling the world's energy needs both now and in the future. Currently, much of the world's energy is provided by coal and petroleum. However, these sources have a negative impact on the environment and are becoming more difficult to extract and purify. Great work has been done in developing alternative solutions (e.g. nuclear, solar, wind and hydroelectric), but these technologies require improvements in energy storage, both to match variable supply to variable demand and to allow this energy to be used in transportation and mobile electronics [1]. Unfortunately, since the advent of lithium ion (Li+) batteries in 1991, there have been only minimal improvements in the storage capacity of batteries [2].

1.1 Conventional Lithium Ion Batteries

A battery cell receives and delivers electrical energy, but the energy is stored chemically. It can be thought of as somewhat analogous to rolling a rock up a hill. At the top of the hill the rock possesses potential energy that can be dispersed by letting it roll down and recharged by rolling the rock back up the hill. In a Li^+ battery, the Li atoms are like the rock. They can be stored in the negative high potential electrode (anode) and allowed to "roll down" to a positive low potential electrode (cathode). The electrodes are separated by an electrolyte that is conductive to Li^+ ions but not to electrons. Consequently, the Li atoms cannot "roll downhill" unless there is a

pathway the extra electron can take to reach the anode. As the electrons move through this path, they supply electrical power. The capacity of the battery is proportional to the number of Li atoms that can be stored in the anode and cathode. Currently, the anode is usually made out of graphitic carbon microspheres [2], used not to optimize capacity, but because they are reliable and retain capacity after many cycles.

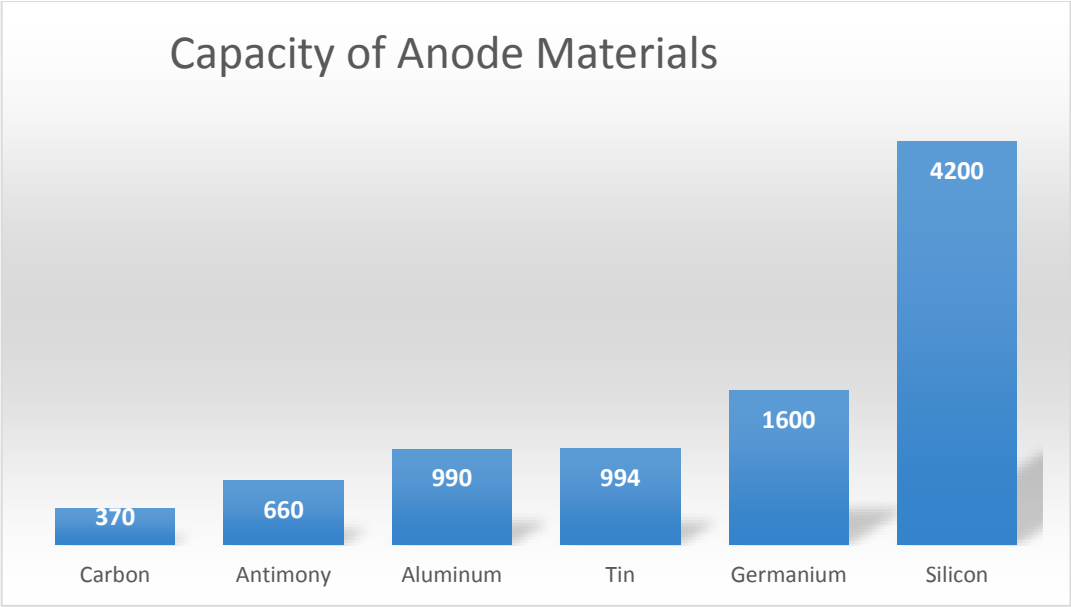

Figure 1-1 Theoretical lithium storage capacities of potential materials for anodes. Capacities are in mAhr/g. Currently, anodes are made of carbon. As seen, silicon offers an order of magnitude improvement.

1.2 Silicon as an Anode Material

Silicon has the highest known theoretical capacity of any anode material, as seen in figure 1-1. It is an order of magnitude greater than graphitic carbon. Furthermore, it is the second most abundant element on earth [3]. Unfortunately, several challenges prevent its use in commercial batteries including capacity fading during cycling (as the cell is charged and discharged the amount of storable energy decreases) and poor rate capability (charging and discharging the cell at higher

currents also decreases the storable energy) [4]. Nanostructures have shown promise to overcoming these challenges [5]. One such example is vertically aligned carbon nanotubes (VACNTs) coated in silicon [6] which can now be mass produced economically [7], [8].

1.3 Contribution of this Work

We present here three studies designed to increase understanding of the problems faced by silicon coated VACNTs (Si-CNT) electrodes and to find solutions. The first study deals with the rate capability or power density of these cells. We search for a variable that limits the usable current and attempt to resolve what the author sees as a disagreement in the literature. The second presents a novel nanoscale monolith as a scaffolding for Si in electrodes. It is fabricated by coating VACNTs in nanocrystalline carbon. Despite the advantages of this monolith, cycle fading is still observed at carbon loadings less than 60% of the electrode volume. At loadings above 60% carbon, stable cycling is observed, and the volumetric capacity of these electrodes is ~1000mAhr/ml. The final study demonstrates a method for increasing stability during cycling by putting a carbon shell or encapsulation layer around the porous silicon electrode. Stable cycling is obtained, but only at silicon loadings less than 5% of electrode volume.

Chapter 2

Understanding Rate Capability of Si-CNT Anodes in Li-Ion Batteries

2.1 Rate Capability

Although silicon has a high energy density, certain applications require a high rate capability or "fast charging." An example of this with regard to transportation would be the time necessary to recharge the battery for an electric car. High rate capability is the ability of a battery to maintain a high percentage of its capacity when it is cycled at higher currents.

There is disagreement in the literature about what causes the poor rate capability of silicon batteries, especially when the electrodes are ultra-thick as can be the case with Si-CNT electrodes,

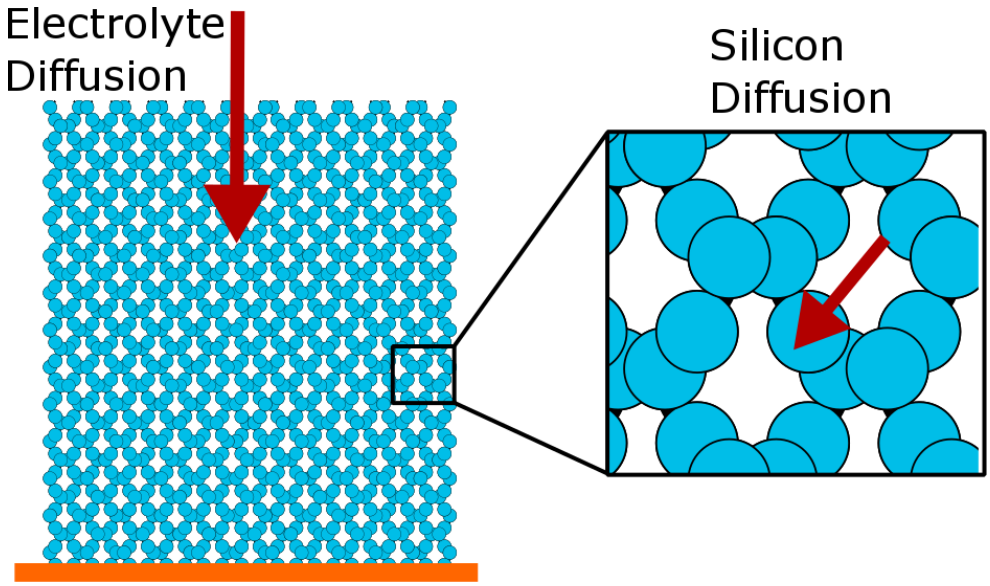

Figure 2-1 Two potential limiting factors for the rate capability of Si-CNT electrodes are presented. Electrolyte diffusion is the diffusion of lithium through the electrolyte into the VACNT forest. This diffusion is fast, but occurs on a length scale of hundreds of microns. Silicon diffusion is the diffusion into the solid silicon nanoparticles deposited on the forest. The diffusion is slow, but occurs on a length scale of just a few nanometers.

which are frequently hundreds of microns thick. Some have proposed, due to this thickness, that Li diffusion through the electrolyte down the VACNT forest limits the viable current [9], [10]; Others argue, the limiting factor is the diffusion of the lithium into the bulk silicon and that the limiting variable is the Si coating thickness [11], [12]. Although this is a much smaller distance, on the order of nanometers, the transport through the solid, amorphous silicon is much slower than in the electrolyte.

Both of these mechanisms are shown in Figure 2-1. To test these ideas, tall (hundreds of microns) electrodes were fabricated with and without an array of 10 μm square pores spaced 10 μm apart. The pores effectively reduce the diffusion length from hundreds of microns to 10 μm. The electrodes were then made into half cells and cycled against lithium foil at a variety of currents, and there was no significant difference in the rate capability of the cells. A similar test was performed with two electrodes (without pores) that had different loadings or densities of silicon and consequently different Si coating thicknesses. These two electrodes showed a marked difference in performance at higher rates, indicating that diffusion into the silicon is the rate limiting factor in Si-CNT electrodes.

2.2 C-Rate

The standard unit of current, charge per unit time, is not ideal for batteries because an electrode with greater capacity will, at the same current, take longer to charge than an electrode with less capacity, effectively charging slower. Instead, battery charging currents are usually reported in C rate, where 1 C is the current predicted to charge the battery in 1 hour. Consequently, a current of C/2 charges a battery in 2 hours and 2C in 30 min.

2.3 Si-CNT Anode Fabrication

The electrode fabrication process is outlined in figure 2-2 and is based on the carbon nanotube microfabrication process outlined in Hutchinson et al. [13]. First, 30 nm of Al_2O_3 is coated onto a silicon wafer by electron beam deposition. Then a patterned layer of 4 nm of Fe is deposited using a lift off process and thermal evaporation. This layer serves as the catalyst for growth of VACNT forests, and the forest only grows where there is catalyst present. The forest is grown by atmosphere CVD decomposition of ethylene at 750 °C, then removed from the wafer by an oxidation process, annealing in 1000 ppm of water for 5-10 minutes immediately after growth, and a mechanical force applied to complete the delamination [14]. The CNTs are coated in silicon

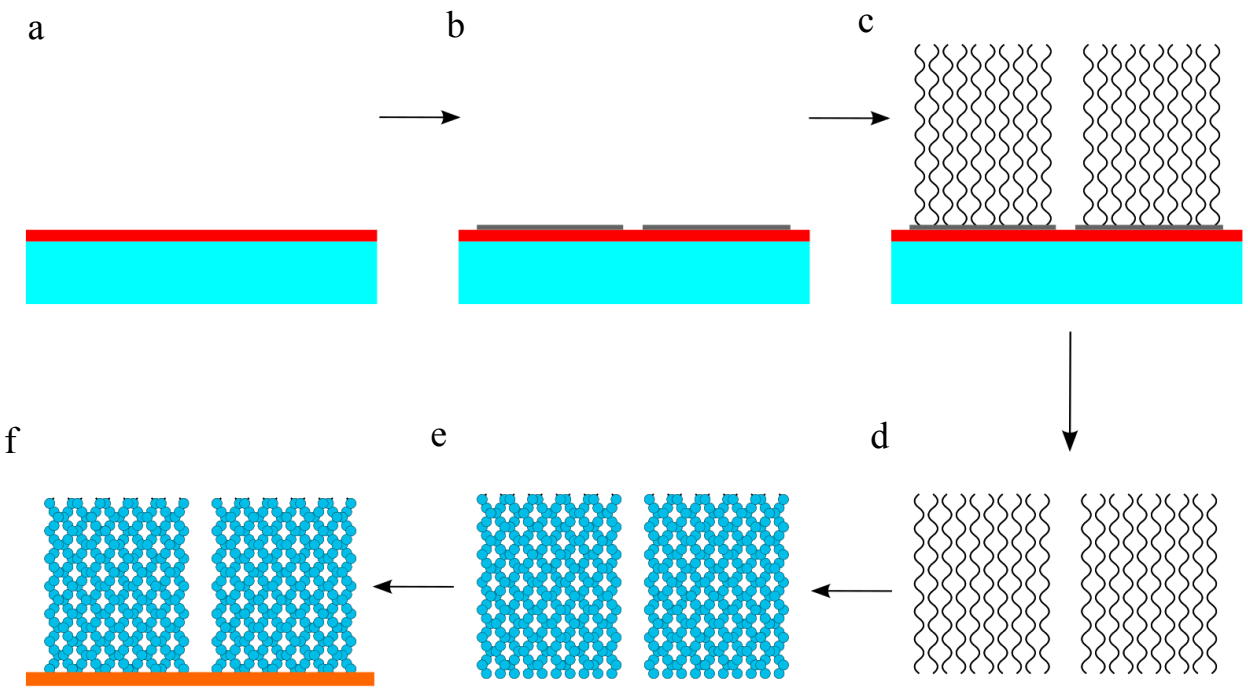

Figure 2-2 Process outline for fabrication of Si-CNT electrodes. a. 30 nm of Al_2O_3 is coated onto a silicon wafer by electron beam deposition; b. a patterned layer of 4 nm of Fe is deposited using a lift off process with thermal evaporation; c. CNT forest is grown from the Fe catalyst by atmosphere CVD decomposition of ethylene at 750 °C; d. structure is removed from wafer by annealing in 1000 ppm of water for 5-10 minutes immediately after growth and a mechanical force is applied to complete the delamination of the forest; e. The forest is filled with a thin layer of silicon by silane decomposition at 550 °C and 200 mtorr; f. An ultra-thin (125 nm) copper current collector is deposited onto the back of the forest by thermal evaporation.

by lpcvd silane decomposition at 550 °C and 200 mtorr. Finally, an ultra-thin (125 nm) copper current collector is deposited onto the back of the forest by thermal evaporation.

An important variable of electrode performance is silicon loading. All loadings will be reported in the percent of the forest volume occupied by the silicon assuming a density of 1.9 g/cm^3. When referring to carbon loadings in this thesis, a density of 2.27 g/cm^3 is assumed.

2.4 Ultra-Thin Copper Current Collectors

As Li-Ion battery capacities increase, the metal foil current collectors, begin to dominate the mass of the electrode, as seen in figure 2-3. A unique characteristic of VACNTs is a thin flat layer on the backside, and ultra-thin current collectors can be deposited on said layer. These layers can weigh dramatically less than copper foils currently because foils cannot be rolled thinner than a few microns. These thinner layers are more resistive, but the thickness can be increased to meet the application.

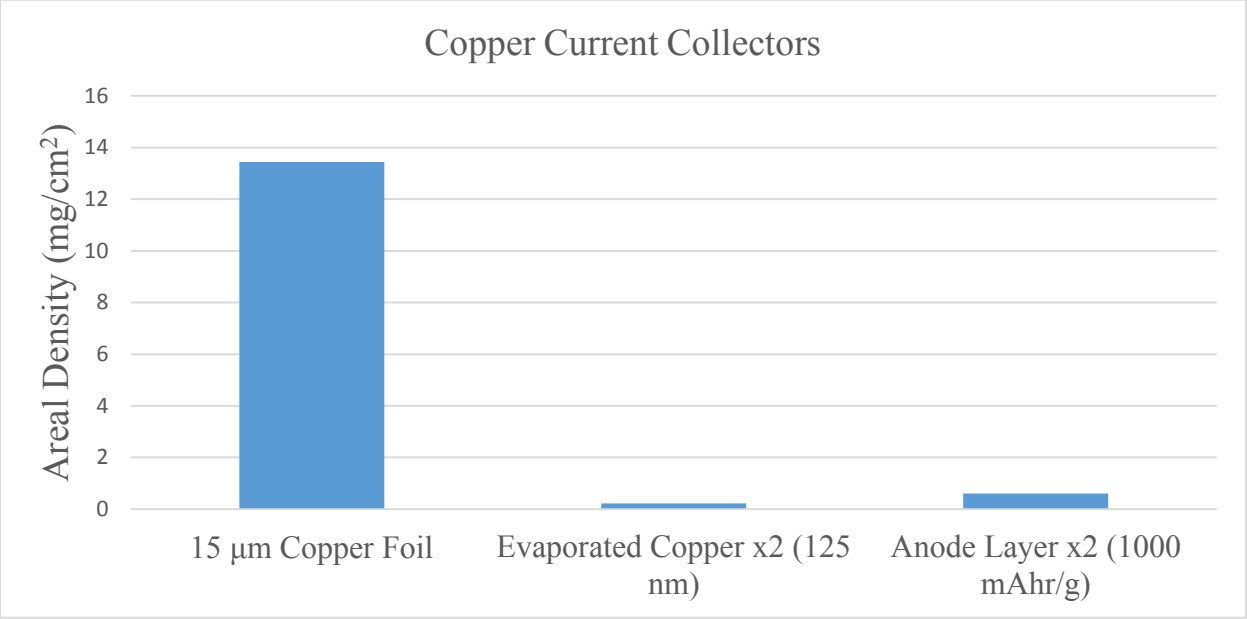

Figure 2-3 Comparison of the mass contributions of foil current collectors and evaporated current collectors. The anode mass and evaporated layer mass are doubled to better compare to the foil which would be coated on both sides in a commercial cell. The anode mass assumes 1000 mAhr/g and 3.7 mAhr/cm^2.

2.5 Electrochemical Testing

Half cells were made using CR2025 coin cells, assembled in an Ar-filled glovebox with less than .8 ppm H_2O and .67 ppm O_2. Cells used 1M LiPF6 in 1:1 ratio of ethylene carbonate/diethyl carbonate electrolyte, two 25 µm Celgard 2400 polypropylene separators, and 15.6 mm diameter, 250 µm Li metal disks (MTI corp.). The cell was compressed by a wave spring.

Cells were charged and discharged between, 0.01V and 0.8V, and rested for 30 min between cycles. They were cycled at C/10 for 3 cycles and C/4, C/2, 1C, and 2C for 5 cycles each. C-rates were based on a silicon capacity of 2.5 Ahr/g.

2.6 Electrolyte Diffusion

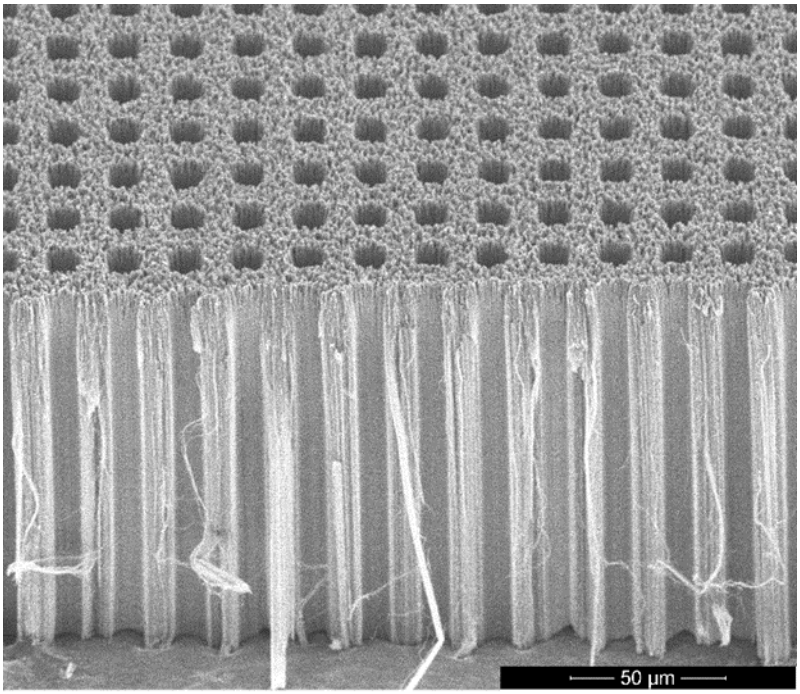

Figure 2-4 Scanning Electron Microscope (SEM) image of a patterned CNT forest. The pattern is an array of 10 µm square holes spaced 10 µm apart. Looking at 45° angle on a broken edge of the forest, the holes are visible, penetrating all the way through the forest.

To test the impact of electrolyte diffusion or rate capability, electrodes with hole arrays (10 µm square pores spaced 10 µm apart as seen in figure 2-4) and electrodes with no hole arrays were grown to 300-400 µm tall. It is important both electrodes have the same silicon loading, otherwise they will have different silicon coating thicknesses. Two cells each with similar silicon loadings (the loading of the hole electrode was 2.13% and the loading of the no hole electrode was 2.17%) were cycled in half cells, as seen in figure 2-5. There was no significant difference in rate capability or capacity retention. This implies the electrolyte diffusion path does not limit the rate capability because if it did the holes would provide much shorter and faster Li transport.

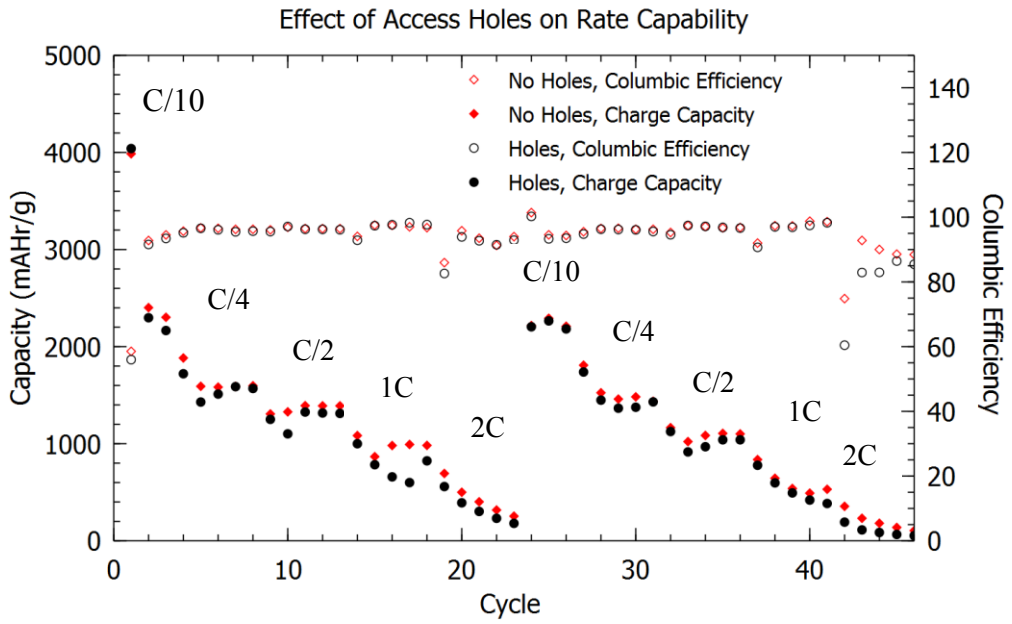

Figure 2-5 Cycling performance of an electrode with an array of holes and an electrode without holes. Both had approximately the same silicon loading, 2.13% and 2.17% respectively. There is no significant difference between the two electrodes in rate capability, implying diffusion through the electrolyte is not the rate limiting mechanism.

2.7 Silicon Diffusion

To test the importance of the diffusion path into the silicon coating, two unpatterned electrodes with different loadings (2.17% and 3.54%) were tested and compared. The results can be seen in figure 2-6. The more lightly loaded electrode (thinner silicon coating) loses less capacity than the more heavily loaded electrode when the C-rate increases to C/2. Since making the silicon thicker decreases the rate capability, the silicon diffusion pathway appears to be the limiting mechanism. A potential implication of this result is that higher densities of CNTs may be able to increase the rate capability of a given cell loading.

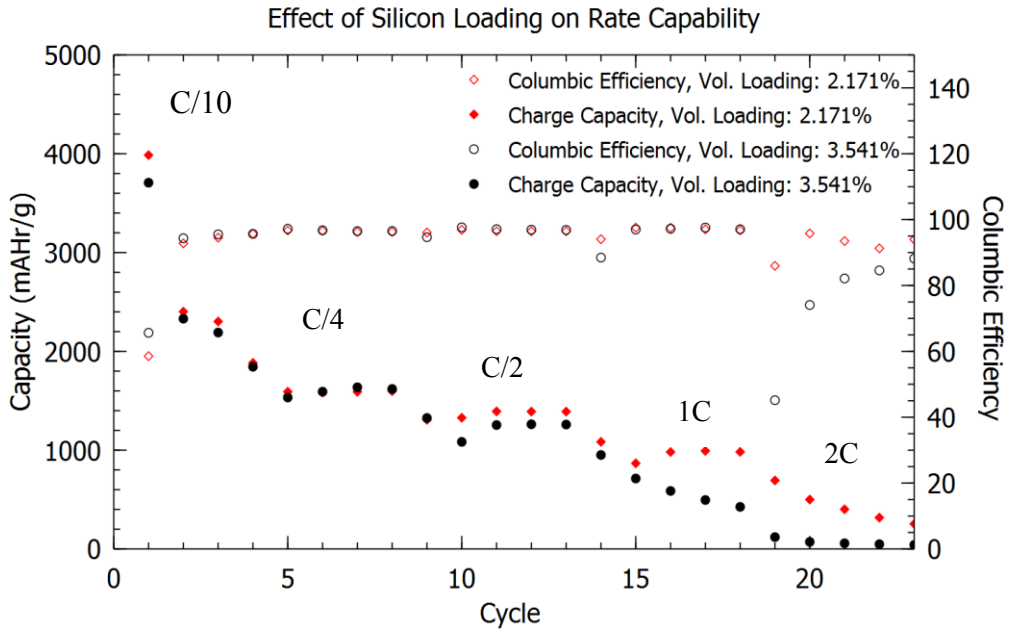

Figure 2-6 Cycling performance of an electrode with a 2.171% Si loading and one with 3.541% silicon loading. The initial capacities are similar, but the heavier cell loses capacity faster at higher rates. This implies Li diffusion into the silicon is the rate limiting factor.

Chapter 3

Silicon-Carbon-CNT Monolithic Anodes: Fabrication, Failure Mechanisms, and Volumetric Capacity

3.1 Cycle Fading of Silicon Anodes

One of the challenges of silicon anodes is that they lose capacity as they are cycled. This has been largely attributed to two phenomenon:

1. Silicon expands as much as 300% when filled with Li which results in mechanical stress gradients that destroy the electrode [15].
2. Anode materials, such as silicon, form an interfacial layer with the electrolyte called the solid/electrolyte interphase (SEI). The SEI layer that forms on carbon is dense and stable which allows for cycling without fading; however, the SEI that forms on silicon is unstable and grows uncontrollably which inhibits good long term cycling [16].

3.2 Expansion Due to Lithiation

Expansion due to lithiation prevents silicon from being stable in the microsphere geometries common to graphitic carbon anodes. Thin films, on the other hand, have been studied and better capacity retention after many cycles has been observed in said films because the small thickness prevents the forces in the film from growing large enough to destroy the electrode [17]. Unfortunately, these thin film batteries have a very small overall capacity because there is little active material. To gain more active material, silicon nanoparticles, silicon nanowires, vertically

aligned carbon nanotubes (VACNTs) coated with silicon [9], [11] and viruses coated with nickel and silicon [18] have all been used. The idea is to gain more active material by putting a thin film of silicon on a scaffolding with an extremely large surface area. For example, CNT's can have the surface area of 5 NBA basketball courts per gram [19].

Nano structuring silicon mitigates the damage caused by stresses during expansion. However, all recently demonstrated anodes have only been able to achieve stable cycling when the anode had a small quantity of silicon. The quantity of silicon that current anodes can hold are all limited, either by the thickness of the silicon layer that can be used before mechanical damage occurs or by the thickness of the electrode that can be used before resistance from the current collector grows too large. For example, silicon coated VACNTs, despite being able to be grown to millimeter heights without significant resistance, show evidence of nanoscale cracking during lithiation, if the silicon layer has significant thickness [20]. Alternatively, nanoparticle architectures allow for high silicon densities, but face resistances that limit the possible thickness of the electrode. Currently, the nanoparticle batteries currently outpreform scaffolding mechanisms, showing stable cycling with areal capacities as high as 3.7 mAhr/cm^2 which is the same level as commercial carbon anodes [21], [22].

3.3 Carbon Coated VACNTs Monoliths

VACNTs provide an excellent scaffolding for silicon because each CNT provides its coating with a direct connection to the current collector [6], and they can be grown millimeters tall without significant resistance. At low loadings (before the tube is completely coated in Si nanoparticles), places where the CNTs contact each other provide extra stability so that if one CNT gets damaged the rest of the material on the CNT still has a conducting pathway to the current

collector. This partially explains why it has been reported that VACNTs coated in silicon perform better when there is still space between the deposited silicon grains [6], [11].

However, there are drawbacks to CNTs. The extra pathways are lost at loadings that cover the entire CNTs. At high loadings CNTs undergo large degrees of motion during lithiation, due to their flexibility. In addition, VACNTs are not compatible with wet processing because the surface tension of the solvent during drying (or even a critical point drier) will destroy the forest.

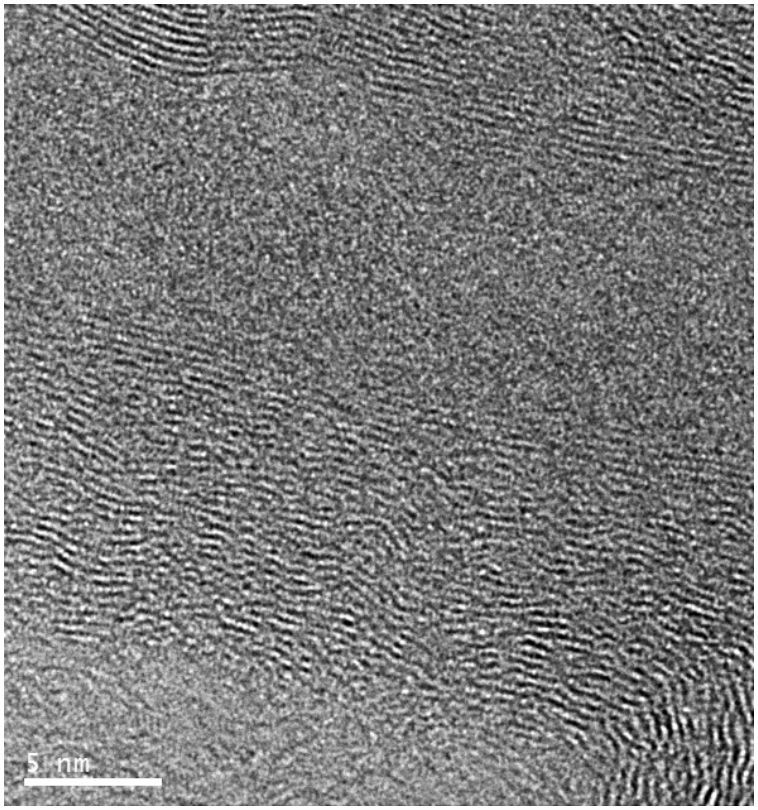

Figure 3-1 Fringe contrast TEM image of a carbon coated carbon nanotube (C-CNT). Straight interior layers are the CNT and the wavy exterior layers are the carbon coating which is not perfectly graphitic.

To overcome these drawbacks, a VACNT monolith structure (C-CNTs) was created depositing an additional layer of nanocrystalline carbon by atmosphere decomposition of ethylene at 900 °C, immediately following growth. This layer, as seen in figure 3-1, conformally coats all of the CNTs and dramatically increases the rigidity of the forest, locking points of contact between

CNTs. This increased rigidity, decreases the deformation of CNTs during lithiation, and also allows the electrode to be wet processed. The nature of the drying needed depends on the duration of the carbon coating. Depositions of 45s or longer can be dried after soaking in a low surface tension solvent such as isopropanol (IPA). Forests coated less than 45s may have to be critical point dried to prevent damage.

Silicon coated C-CNTs (Si-C-CNTs) still exhibit capacity fade with cycling. Some of the fade can be attributed to SEI build up decreasing the ionic conductivity of the electrode. However, it also appears that the silicon can delaminate from the C-CNT scaffolding during lithiation. More stability can be found when measures are taken to decrease the expansion of the silicon, including increasing the carbon loading to greater than 60% of the electrode volume.

3.4 Fabrication

Fabrication of Si-C-CNT electrodes is similar to the process outlined in figure 2-2. The only difference is that the nanocrystalline carbon coating is applied after growth, and the structure is removed from the wafer by etching in KOH at 70 °C for approximately 1 hour, instead of the water based oxidation step used on VACNTs.

Additionally, to study high loading and to do so at high rates (to obtain many cycles quickly), it was necessary to decrease the height of the electrodes to 15-30 μm because there is a limit to the current density at which Li metal can cycle stably (the cut off is between 1-1.5 mA/cm^2) [23].

3.5 Electrochemical Testing

The battery assembly is the same as outlined in section 2-5, with a few minor changes. Cells are cycled between .01-1V. An additive of 2% vineylene carbonate (Sigma Aldrich) by

volume was added to the electrolyte, and cells are cycled at C/2 with a C/10 first cycle unless otherwise noted.

Differential capacity curves required significant noise reduction. The voltage vs. capacity data was interpolated with third order polyharmonic splines and an S value (smoothing value) of 10^{-7}, using "polyharmonic_splines.jl" in Julia. The derivative of the interpolated function was taken at equally spaced points and plotted using the Winston package in Julia.

3.6 Silicon Delamination

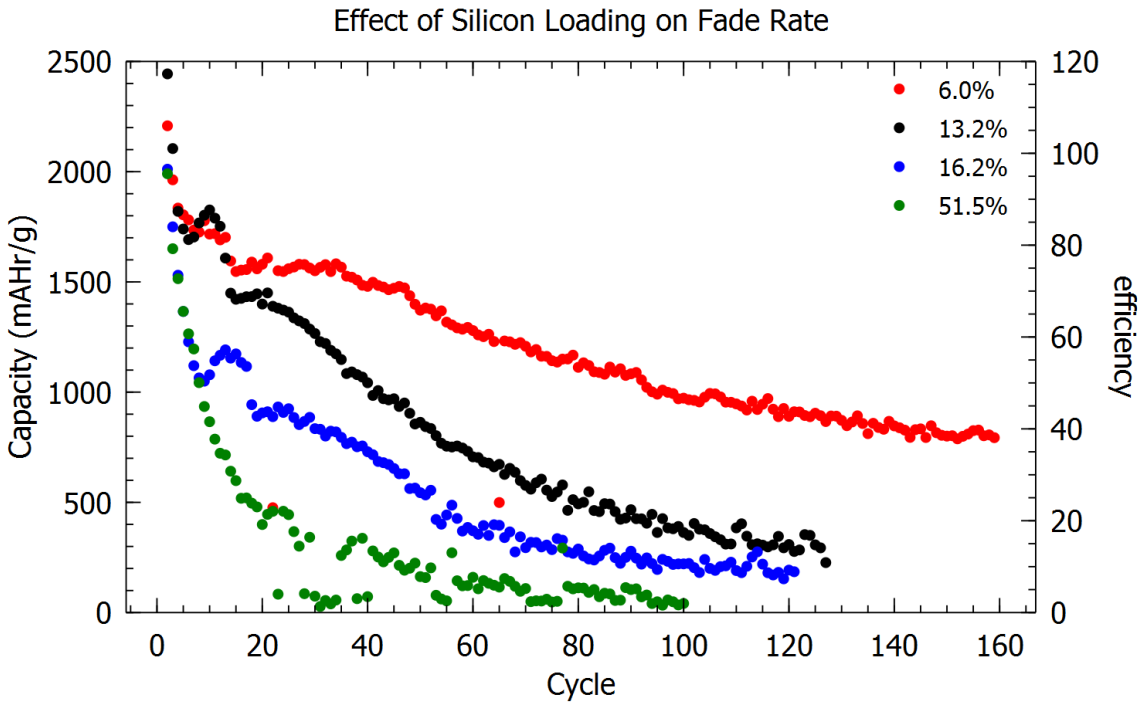

Figure 3-2 Effect of different levels of silicon loading on cycling. All cells are cycled at C/2 with a first conditioning cycle at C/10.

After cycling many cells, it was discovered that the fade rate was strongly dependent on silicon loading, as seen in figure 3-2. This dependency seems to indicate a failure mechanism that is based on silicon expansion, not just unstable SEI formation. This indication seems to be

confirmed by the differential capacity of charging electrodes. If SEI was responsible for the failure, one might expect to see the position of the lithiation peak at .2 V to decrease as the ionic conductivity of the cell decreases and a voltage drop occurs across the SEI.

As seen in figure 3-3, this mechanism is present; however, there is also a decrease in peak intensity that begins many cycles before the peak position begins to change. This change is attributed to delamination of silicon from the C-CNTs scaffolding. This can be observed in figure 3-4. This figure shows TEM images of cells after cycling. The samples were prepared by rinsing in DEC to remove the solvent, and etching in concentrate HCl for 1 hour to remove the SEI. There were sections on the resulting sample, where no silicon could be measured by energy dispersive X-ray spectroscopy (XEDS). In these areas (figure 3-4 a,b), black nanocrystalline sections can be seen peeling off the CNT base. Additionally, there is a large thin amorphous layer that may represent delaminated CNT walls.

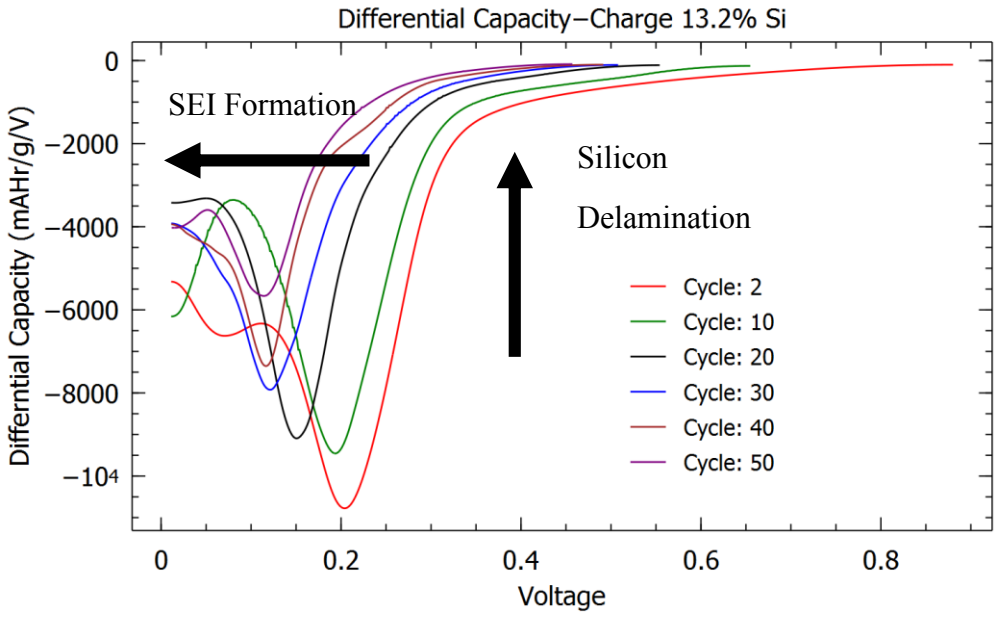

Figure 3-3 Charge side of the differential capacity plot for a 13.2% silicon electrode (the cycling is shown in figure 3-2) The main silicon lithiation peak both loses intensity and shifts to a lower potential. The authors attribute the decrease in intensity to active material being lost when silicon nanoparticles delaminate from the scaffolding due to expansion. The position change is attributed to an increase in ionic conductivity on the charge side due to solid electrolyte interphase (SEI) formation.

3.7 Expansion Suppression

To confirm this theory two methods were attempted to decrease expansion and increase the stability of the cycling. First, a cell was cycled without the conditioning cycle. The C/10 conditioning cycle gains more reversible capacity and therefore a greater degree of expansion than the subsequent C/2 cycles. As seen in figure 3-5, removing this cycle allows the electrode to cycle more stably than even electrodes with significantly lower loadings.

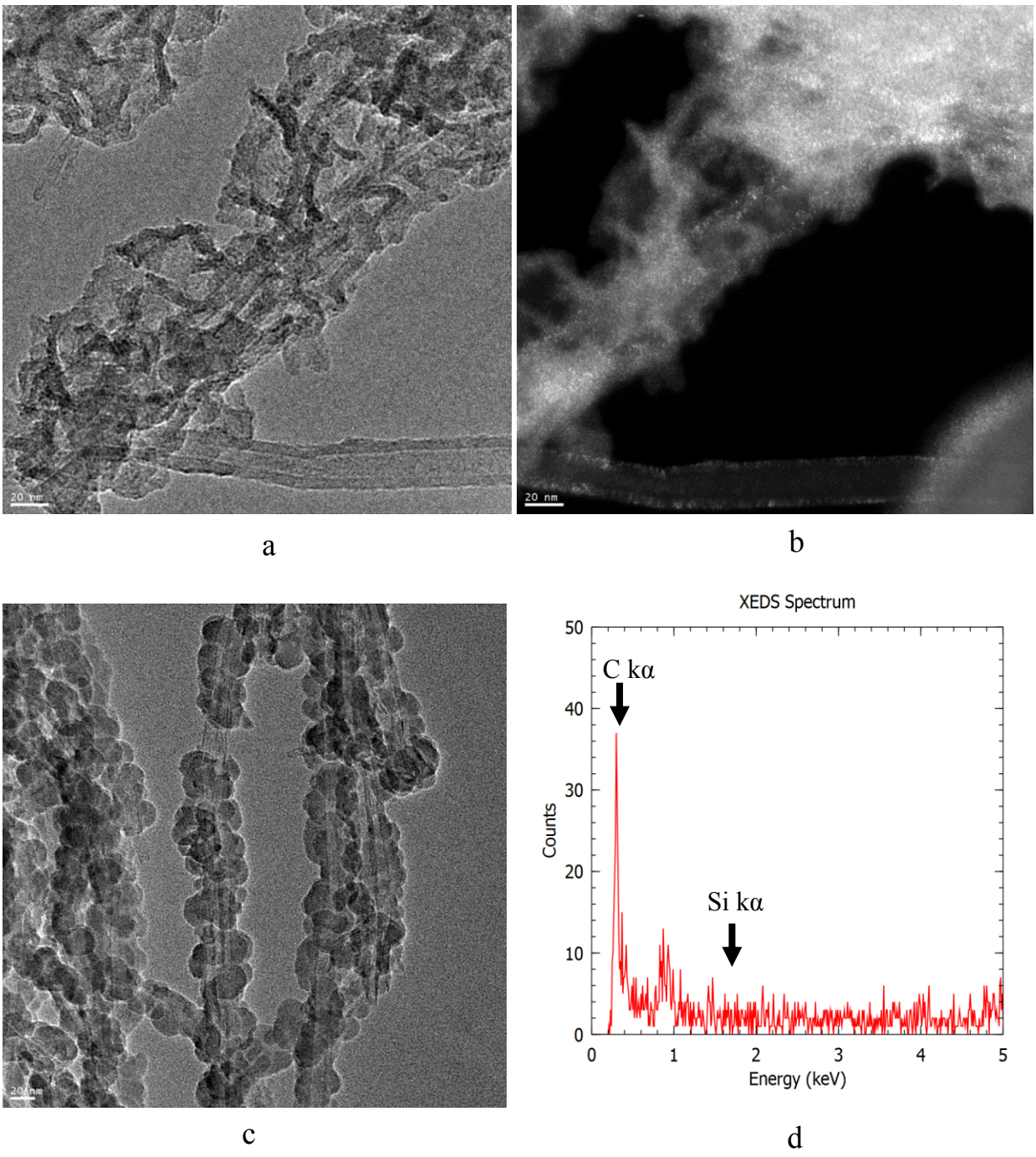

Figure 3-4 TEM analysis on heavily loaded Si-C-CNT. a. Bright field (BF) TEM image of a heavily loaded battery after about 100 cycles, SEI was removed with concentrated HCl acid before imaging. b. Dark field image of the same section. c. BF image of a heavily loaded Si-C-CNT electrode before cycling. d. Energy dispersive x-ray spectrum for a point on the same tube as a. and b. It shows a carbon k alpha peak, but no silicon k alpha peak. The authors conclude that the silicon has torn the carbon coating and delaminated from the structure. Other areas on the same sample as a, b, and d still had significant quantities of silicon remaining.

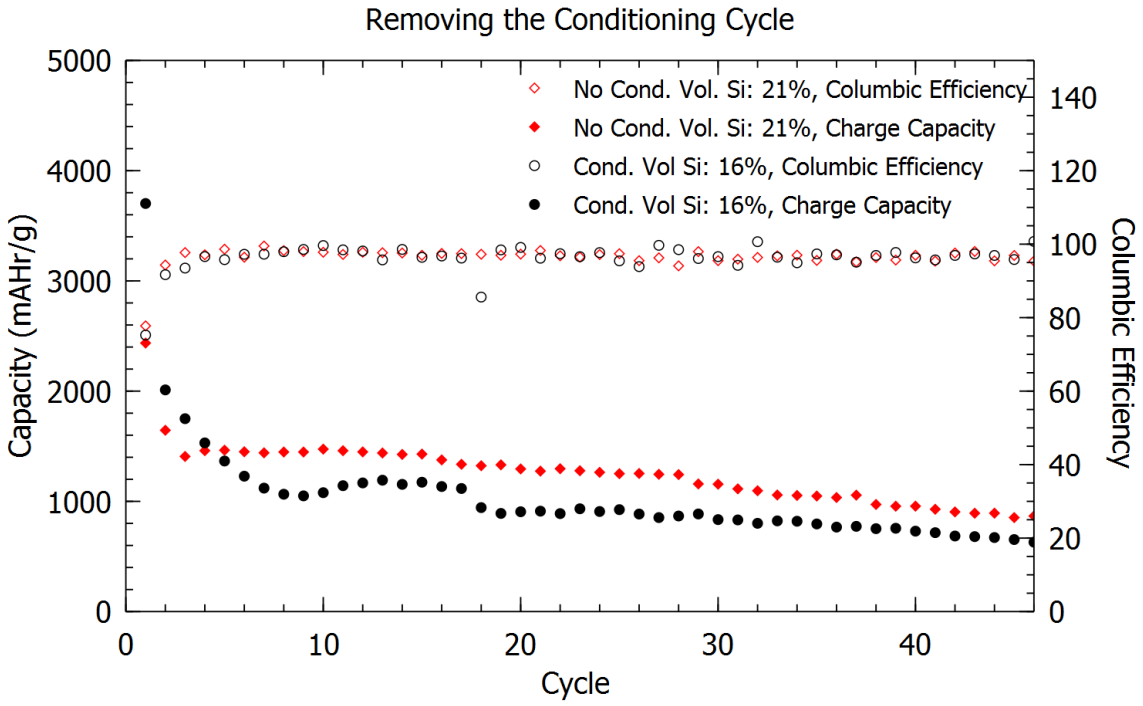

Figure 3-5 Comparison of the charge capacity and columbic efficiency during cycling of two different electrodes. One with a higher silicon loading (21% by volume) and no C/10 conditioning cycle. The second has a lower silicon loading (16% by volume) and a C/10 conditioning cycle. The second fades faster. This is attributed to the lower capacity and significantly decreased expansion of the first cycle.

Second, a Si-C-CNT structure with a much larger carbon loading was prepared. The loading was almost 65% compared to 5-20% in standard cells. This cell was able to achieve stable cycling, as seen if figure 3-6, even at a silicon loading of ~30%. Unfortunately, the silicon is only about 30% of the mass of the electrode as well, but despite its low mass capacity the electrode has a volumetric capacity of ~1000 mAhr/ml.

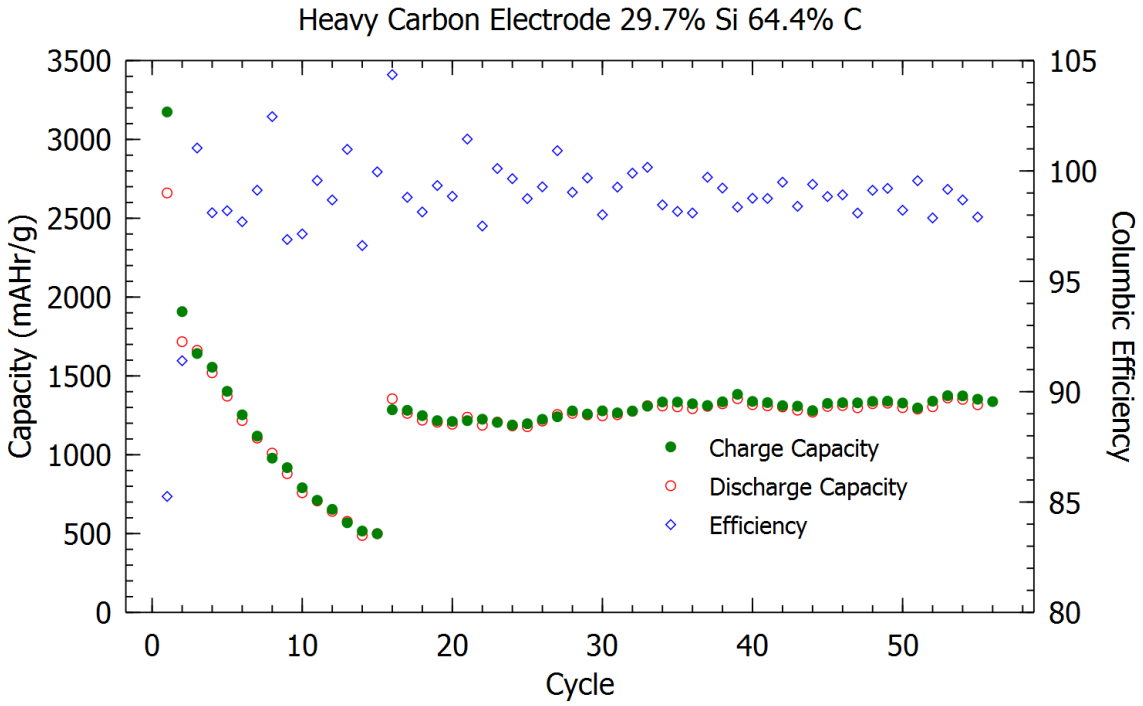

Figure 3-6 Cycling results of an electrode cycled at C/2 with a first cycle at C/10. Estimated capacity due to carbon has been removed and the remaining capacity was normalized by the mass of Si. Carbon capacity was estimated to be 120 mAhr/g based on cycling of C-CNT scaffolding without silicon. The electrode had a dramatically higher carbon loading on the C-CNT scaffolding (64.4% on this electrode vs 5-20% on most electrodes). The electrode also has a high silicon loading (29.7%), but cycles stably after the 15th cycle. This is attributed to the scaffolding being strong enough to prevent the silicon from tearing it apart. The jump up at the 15th cycle is attributed to an unknown effect in the SEI on the Li metal because the current density is a high 1.23 mA/cm^2 and the differential capacity discharge peak shifts to higher voltages during the first 15 cycles (a phenomenon common to cells with current densities higher than the lithium metal threshold of 1-1.5 mA/cm^2), then reverses at cycle 16.

Chapter 4

Encapsulation of VACNTs to Stabilize SEI and Exclude Electrolyte

4.1 Solid Electrolyte Interphase (SEI)

Anode materials (such as silicon) form an interfacial layer with the electrolyte called the solid/electrolyte interphase (SEI). The SEI layer that forms on carbon is dense and stable which allows for cycling without fading. However, the SEI that forms on silicon is unstable and grows uncontrollably which inhibits good long term cycling [15]. Even the silicon anodes that have shown stable cycling, required an extra layer to prevent cycle fading due to the growth of an unstable SEI layer on the silicon. Usually, the extra layer is a thin coating of carbon [9], [24], [25].

4.2 Electrolyte Exclusion

To allow for expansion, Si anodes are porous. If the anode is designed to allow full expansion (~300%), at least 66% of the electrode must be void space. This space becomes filled with electrolyte during assembly which transforms to SEI during cycling. This electrolyte has a density of 1.26 g/cm^3 [26], meaning that its presence reduces the practical mass capacity of the anode by 57%, effectively, turning a 2500 mAhr/g electrode into a 1075 mAhr/g electrode. Consequently, a method that excludes the electrolyte from the interior of the porous anode and stabilizes the SEI is required for Si anodes to reach their maximum capacity.

Here, we report an electrode design that stabilizes the SEI and excludes the electrolyte from the interior of the electrode, called encapsulation. It is the application of a thin shell of carbon to the exterior of the electrode. Although unable to stabilize the cycling of heavily load Si-C-CNT electrodes, it shows promise with lightly loaded electrodes.

4.3 Fabrication

Fabrication of an encapsulation shell that covers the top of a VACNT forest can be achieved by a variety of methods. However, patterning of the forest has several advantages including: allowing the electrode to be made of isolated compartments so that if one is broken the others remain uncompromised and using patterns that increase the mechanical flexibility of the electrode. Encapsulation of patterned forests is more difficult. Some deposition techniques deposit on the exterior of porous structures (e.g. spraying CNTs, evaporation, PECVD) and others (CVD, ALD, certain forms of electroplating) penetrate into the same structures. Unfortunately, due to their combination of micro and nanostructure, patterned CNT forests cannot be coated by any of the

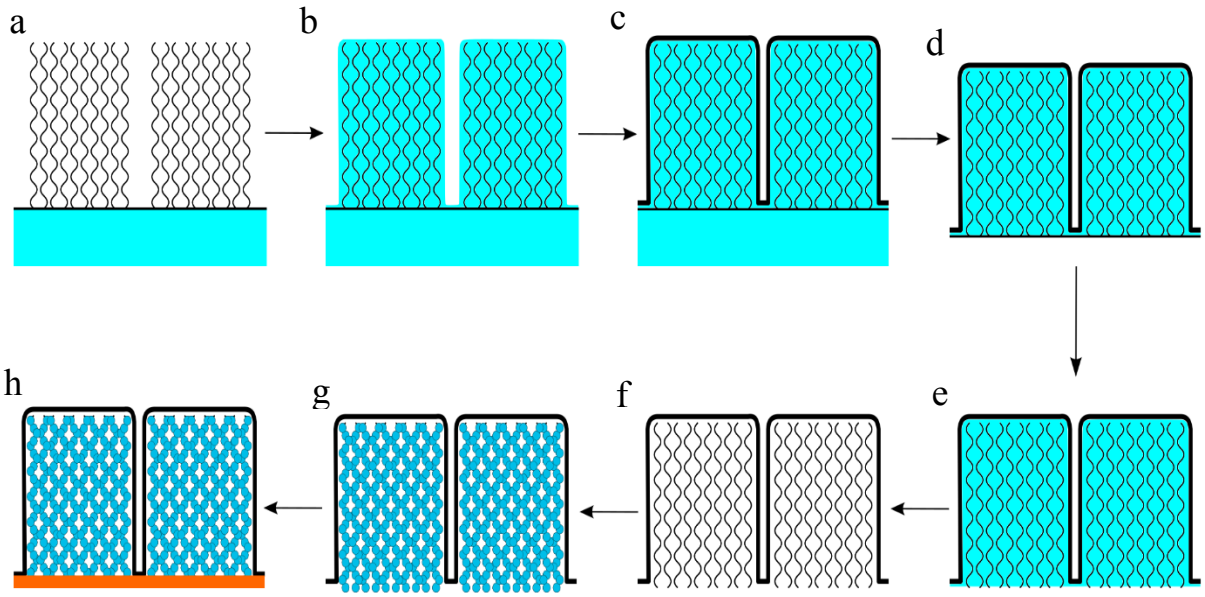

Figure 4-1 Process outline for building electrodes. a. CNT forest is grown and coated with a thin layer of carbon by atmosphere CVD decomposition of ethlyene; b. forest is filled with silicon by lpcvd decomposition of silane; c. silicon structure is coated in carbon by atmosphere CVD decomposition of ethylene.; d. structure is removed from wafer, if it does not happen naturally due to stress it is accomplished by etching in KOH; e. the back floor layer of carbon is removed with an oxygen plasma etcher to provide access for the etchant; f. silicon is selectively removed from the forest by etching with 70 °C KOH for 1 hour; g. The forest is filled with a thin layer of silicon by lpcvd decomposition of silane; h. the back is closed off by thermally evaporating a 600 nm thick copper layer which also serves as a current collector.

above methods because the methods that do not penetrate only coat the top of the microstructure and penetrating methods coat the microstructure but also the nanostructure.

As outlined in figure 4-1, a sacrificial etch method overcomes this limitation, encapsulating patterned CNT forests. A multistep process, this method can best be understood with a simple overview: Using a penetrating CVD process, the forest is filled solid with silicon, removing the nanostructure while maintaining the microstructure, as seen in figure 4-2. CVD, a penetrating process, coats the microstructure in carbon, without fearing it will penetrate into the nanostructure, and the silicon is selectively removed by etching in KOH. The CNTs are then coated in amorphous silicon, the active material.

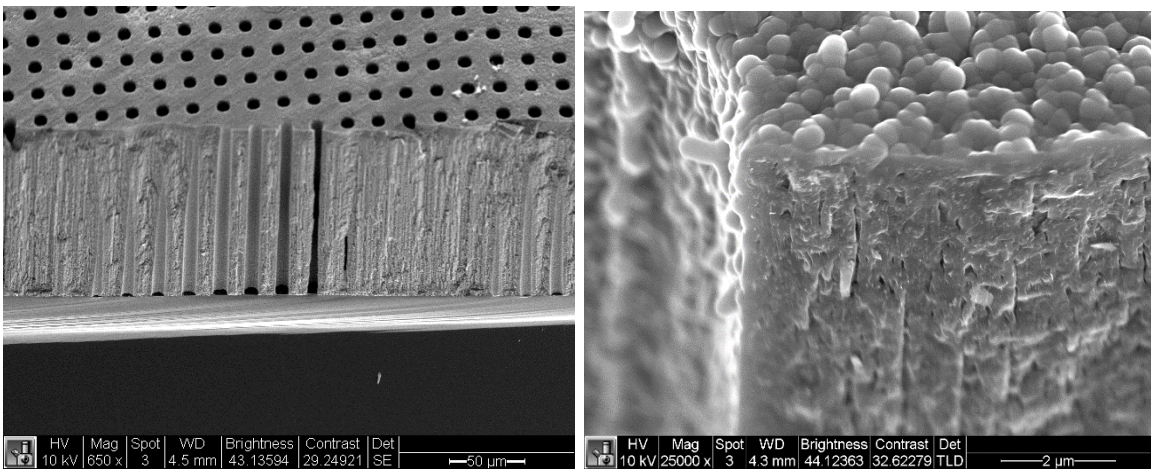

a b

Figure 4-2 SEM images of a patterned CNT forest that has been filled solid by silane decomposition at 585 °C for 1 hour, imaged at 45° a. low and b. high magnification.

Delving into the details, a 30 nm alumina layer is first deposited on a silicon wafer by ebeam evaporation. Then, using a lift off process, 4 nm of iron is patterned on top of the alumina.

A VACNT forest is grown from this catalyst at 750 °C in a tube furnace where hydrogen and ethylene are flowing. The CNTs are also coated in an additional thin carbon layer to add structural stability. This process is done in the same furnace at 900 °C with the same gases flowing.

The forest is placed in a low pressure chemical vapor deposition (lpcvd) system where the tubes are coated with silicon by silane decomposition at 585 °C and 200 mtorr for 60 min. This coating fills in all of the space between tubes and makes the forest a solid block of silicon in the same pattern as the iron catalyst, as seen in figure 4-2. Now, using the process that was used to coat the CNTs with carbon a thick (100+ nm) carbon layer is applied to the outside of the silicon. This is the encapsulation layer.

At this point, due to stress in the deposited carbon and silicon the electrode delaminates from the wafer. If it does not, it can be released be etching in KOH at 70 °C. The bottom of the sample has a thin floor layer of carbon that prevents the KOH from reaching the silicon. This floor layer is removed by etching from approximately 15 min in an O_2 plasma at 200 W and 400-500 mtorr. Now, the backside is open to the CNT forest filled with silicon, and the silicon can be removed by KOH etching at 70 °C for at least one hour. After the etch the sample is soaked for at least 30 min in water to remove the KOH and then soaked for a short time in IPA because IPA has lower surface tension and consequently IPA soaks make the drying process less destructive.

The sample is now a CNT forest with an encapsulation layer, a scaffolding for the active material. The CNTs can now be coated with silicon by lpcvd silane decomposition at 535 °C. Finally, the backside is closed off by evaporating 600 nm of copper. Additionally, this copper layer serves as a lightweight current collector. Figure 4-3 shows the back of the forest before and after copper deposition.

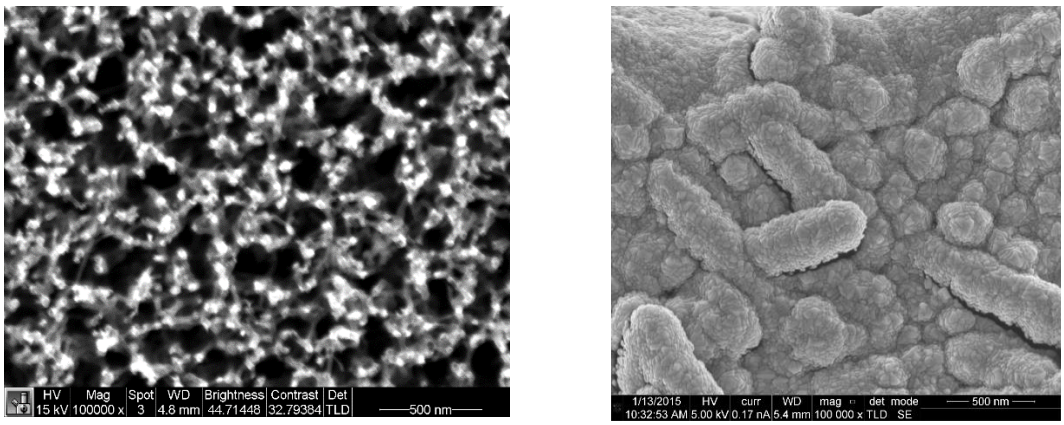

a b

Figure 4-3 SEM images of the backside of the electrode a. before and b. after evaporating a 600 nm copper layer. The copper appears to have sealed the backside of the electrode.

4.4 Electrochemical Testing

Electrochemical testing was performed as outlined in section 3.5.

4.5 Results

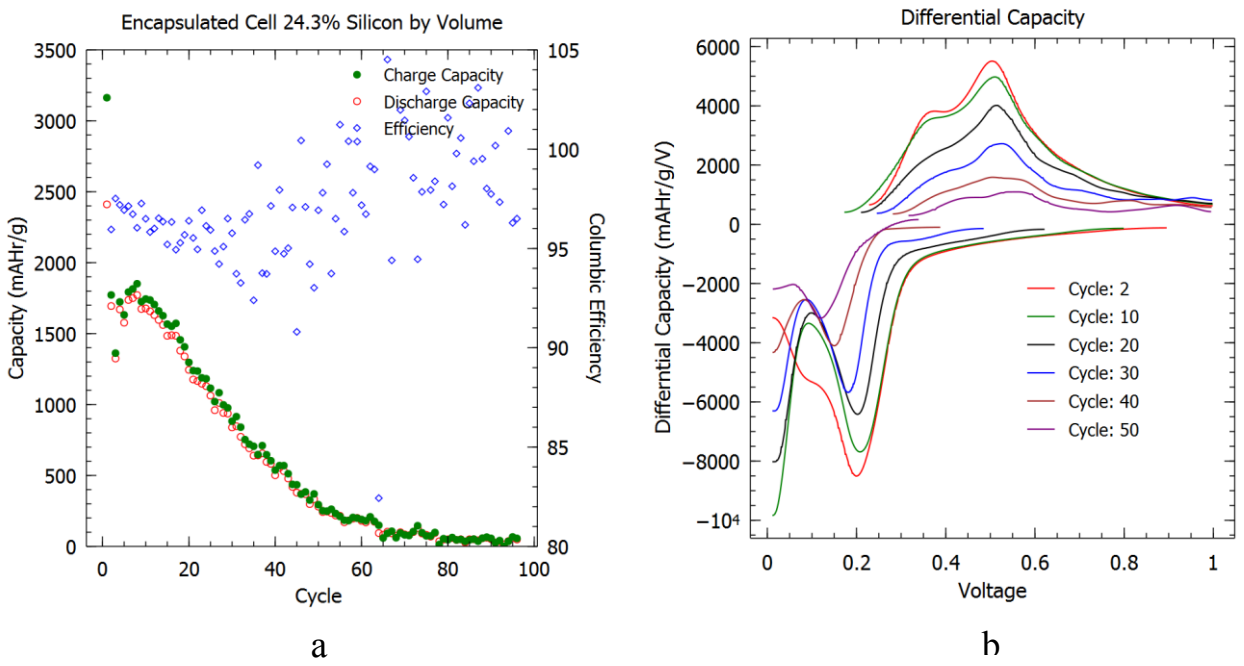

Figure 4-4 a. Cycling results for an encapsulated electrode cycled at C/2 with 24.3% silicon by volume. The electrode is only 18.7 um tall to avoid a current density higher than 1 mA/cm^2. Estimated capacity due to carbon has been removed and the remaining capacity was normalized by the mass of Si. Carbon capacity was estimated to be 120 mAhr/g based on cycling of C-CNT scaffolding without silicon. b. Differential capacity plots for the cycles: 2, 10, 20, 30, 40, and 50. Peak intensity drops due to silicon delamination are visible in all cycles, and peak shifting due to SEI formation is apparent but only after cycle 20.

As seen in figure 4-4, heavily loaded encapsulated samples did not show stability beyond ~10 cycles at C/2. The differential capacity curves show evidence of silicon delamination in all of the cycles and SEI formation after cycle 20. The SEI formation is attributed to fracturing of the encapsulation layer in some areas of the heavily loaded encapsulated samples, as seen in figure 4-5. Other areas appear to remain intact and still maintain porosity after cycling, as seen in figure 4-6.

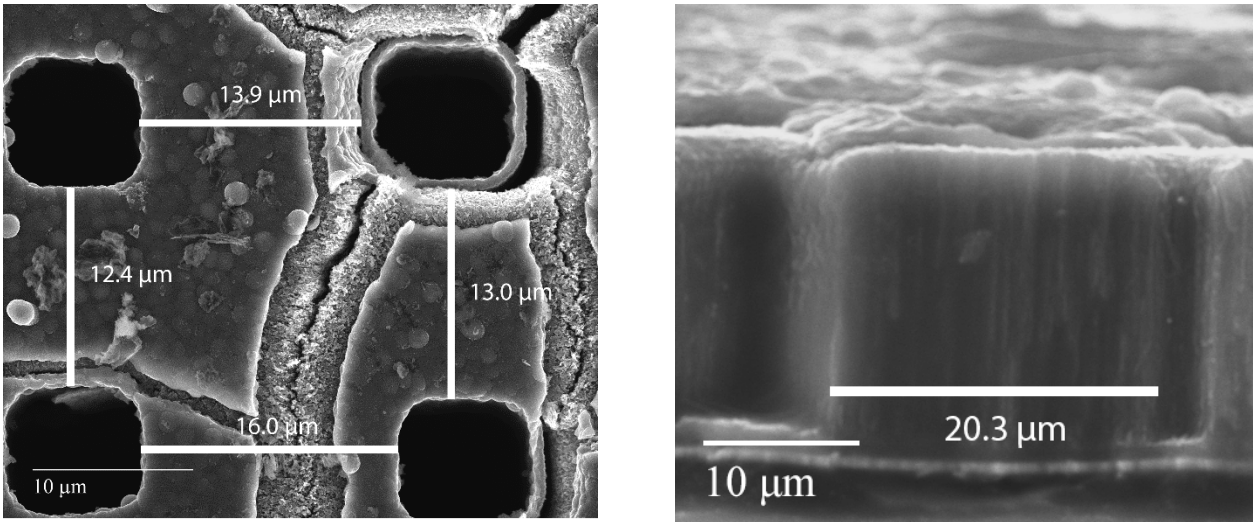

a b

Figure 4-5 SEM images of a. the top of an encapsulated sample after cycling. The encapsulation layer has cracked due to expansion. The original spacing between holes was 10 µm minus the thickness of the encapsulation layer and SEI (~0.75 µm). b. A cross-sectional view of a fractured section of the forest. The forest in that area has become filled with what appears to be SEI. It has also expanded to over twice the original thickness.

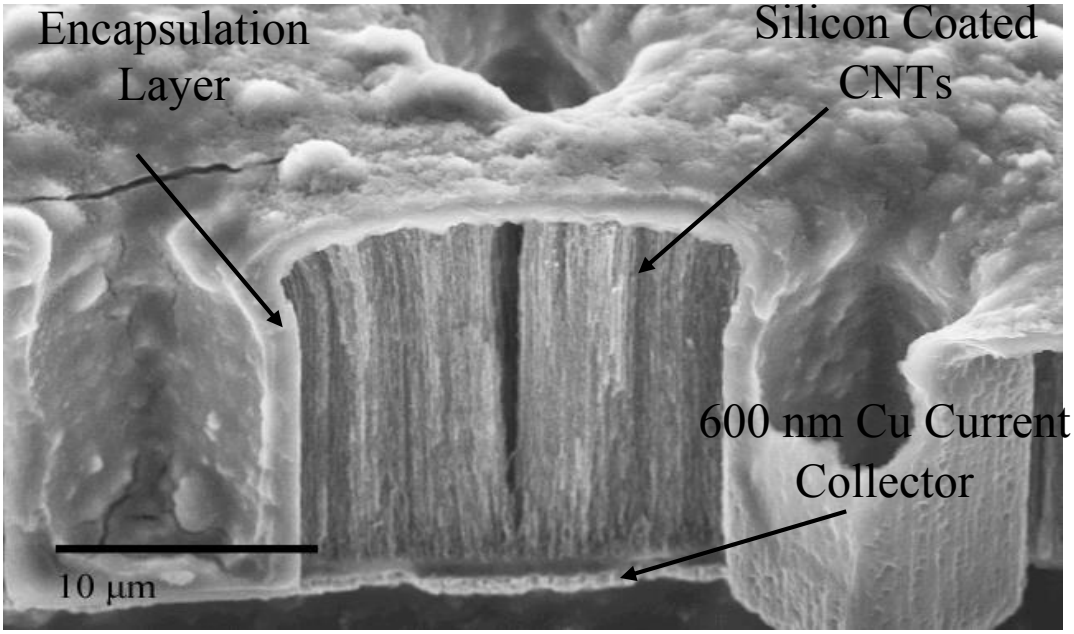

Figure 4-6 SEM image of an encapsulated cell post cycling, looking 45° at a cross-section. The carbon encapsulation layer, Si-C-CNTs, and the 600 nm Cu current collector are all clearly visible.

Electrodes with loadings of less than 5% showed stability when cycled at C/10, figure 4-7, even when ~100 µm tall. Because these electrodes can be tall, it may be possible to use this method to fabricate batteries with a high mass capacity despite their low volume capacity. Such batteries can find application in the transportation industry where low mass capacity is the more important metric.

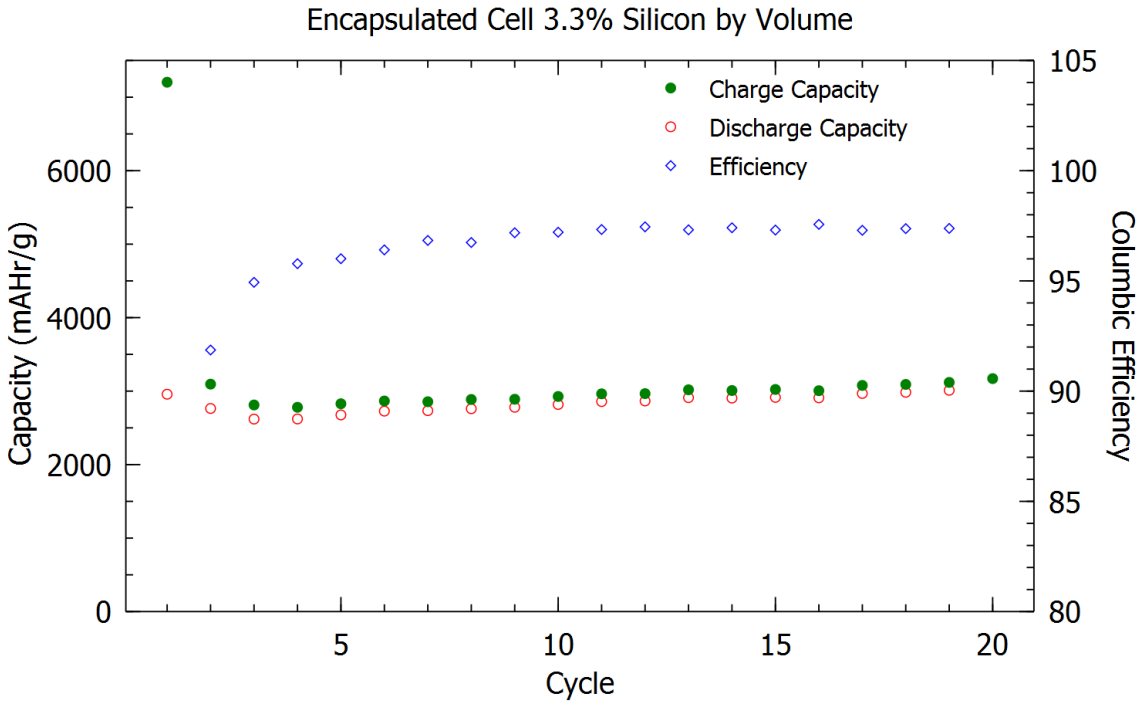

Figure 4-7 Cycling of an encapsulated cell cycled at C/10. The electrode has a height of 95 µm and is 3.3% silicon by volume. Stability can be obtained with low silicon loading and currents. Estimated capacity due to carbon has been removed and the remaining capacity was normalized by the mass of Si. Carbon capacity was estimated to be 120 mAhr/g based on cycling of C-CNT scaffolding without silicon.

Chapter 5

Conclusion

Si-CNT anodes have the potential to dramatically increase the capacity of modern Li-ion batteries. Yet, several challenges remain including the low rate capability of Si-CNT based batteries. In chapter 2, it was demonstrated that the diffusion of Li into the solid silicon coating limits the rate capability.

Capacity fade with cycling also inhibits the application of these electrodes. In chapter 3, a monolith scaffolding was demonstrated, to allow for greater loadings of silicon. It was found that capacity fade of these electrodes came from silicon delamination from the scaffolding as well as SEI formation. They can obtain stable cycling, but only when there is high loadings of carbon to suppress the silicon expansion. This creates an electrode with high volumetric capacity, but low mass capacity. In future work, methods for increasing the strength of the monolith will be examined.

In chapter 4, an encapsulation method that both stabilizes the SEI and excludes the electrolyte from the porous electrode to remove significant amounts of mass in electrolyte was demonstrated. These cells where not stable at high mass loadings, but were stable at low mass loadings even at significant heights. High mass capacities with low volumetric capacities are possible with this configuration, and may have application in the transportation industry.

References

[1] M. M. Thackeray, C. Wolverton, and E. D. Isaacs, "Electrical energy storage for transportation—approaching the limits of, and going beyond, lithium-ion batteries," *Energy Environ. Sci.*, vol. 5, no. 7, p. 7854, Jun. 2012.

[2] M. Armand and J.-M. Tarascon, "Building better batteries.," *Nature*, vol. 451, no. 7179, pp. 652–7, Feb. 2008.

[3] U. Kasavajjula, C. Wang, and A. J. Appleby, "Nano- and bulk-silicon-based insertion anodes for lithium-ion secondary cells," *J. Power Sources*, vol. 163, no. 2, pp. 1003–1039, Jan. 2007.

[4] B. Peng, F. Cheng, Z. Tao, and J. Chen, "Lithium transport at silicon thin film: barrier for high-rate capability anode.," *J. Chem. Phys.*, vol. 133, no. 3, p. 034701, Jul. 2010.

[5] P. G. Bruce, B. Scrosati, and J.-M. Tarascon, "Nanomaterials for rechargeable lithium batteries.," *Angew. Chem. Int. Ed. Engl.*, vol. 47, no. 16, pp. 2930–46, Jan. 2008.

[6] W. Wang, R. Epur, and P. N. Kumta, "Vertically aligned silicon/carbon nanotube (VASCNT) arrays: Hierarchical anodes for lithium-ion battery," *Electrochem. commun.*, vol. 13, no. 5, pp. 429–432, May 2011.

[7] Q. Zhang, J.-Q. Huang, M.-Q. Zhao, W.-Z. Qian, and F. Wei, "Carbon nanotube mass production: principles and processes.," *ChemSusChem*, vol. 4, no. 7, pp. 864–89, Jul. 2011.

[8] M. F. L. De Volder, S. H. Tawfick, R. H. Baughman, and A. J. Hart, "Carbon nanotubes: present and future commercial applications.," *Science*, vol. 339, no. 6119, pp. 535–9, Feb. 2013.

[9] K. Evanoff, J. Khan, A. A. Balandin, A. Magasinski, W. J. Ready, T. F. Fuller, and G. Yushin, "Towards ultrathick battery electrodes: aligned carbon nanotube-enabled architecture.," *Adv. Mater.*, vol. 24, no. 4, pp. 533–7, Jan. 2012.

[10] A. Magasinski, P. Dixon, B. Hertzberg, A. Kvit, J. Ayala, and G. Yushin, "High-performance lithium-ion anodes using a hierarchical bottom-up approach.," *Nat. Mater.*, vol. 9, no. 4, pp. 353–8, May 2010.

[11] A. Gohier, B. Laïk, K.-H. Kim, J.-L. Maurice, J.-P. Pereira-Ramos, C. S. Cojocaru, and P. Van Tran, "High-rate capability silicon decorated vertically aligned carbon nanotubes for Li-ion batteries.," *Adv. Mater.*, vol. 24, no. 19, pp. 2592–7, May 2012.

[12] A. Gohier, B. Laïk, J.-P. Pereira-Ramos, C. S. Cojocaru, and P. Tran-Van, "Influence of the diameter distribution on the rate capability of silicon nanowires for lithium-ion batteries," *J. Power Sources*, vol. 203, pp. 135–139, Apr. 2012.

[13] D. N. Hutchison, N. B. Morrill, Q. Aten, B. W. Turner, B. D. Jensen, L. L. Howell, R. R. Vanfleet, and R. C. Davis, "Carbon Nanotubes as a Framework for High-Aspect-Ratio MEMS Fabrication," *J. Microelectromechanical Syst.*, vol. 19, no. 1, pp. 75–82, Feb. 2010.

[14] L. Ci, S. M. Manikoth, X. Li, R. Vajtai, and P. M. Ajayan, "Ultrathick Freestanding Aligned Carbon Nanotube Films," *Adv. Mater.*, vol. 19, no. 20, pp. 3300–3303, Sep. 2007.

[15] H. Wu and Y. Cui, "Designing nanostructured Si anodes for high energy lithium ion batteries," *Nano Today*, vol. 7, no. 5, pp. 414–429, Oct. 2012.

[16] B. Scrosati and J. Garche, "Lithium batteries: Status, prospects and future," *J. Power Sources*, vol. 195, no. 9, pp. 2419–2430, May 2010.

[17] H. Jung, M. Park, S. H. Han, H. Lim, and S.-K. Joo, "Amorphous silicon thin-film negative electrode prepared by low pressure chemical vapor deposition for lithium-ion batteries," *Solid State Commun.*, vol. 125, no. 7–8, pp. 387–390, Feb. 2003.

[18] X. Chen, K. Gerasopoulos, J. Guo, A. Brown, C. Wang, R. Ghodssi, and J. N. Culver, "Virus-enabled silicon anode for lithium-ion batteries.," *ACS Nano*, vol. 4, no. 9, pp. 5366–72, Sep. 2010.

[19] T. Hiraoka, A. Izadi-Najafabadi, T. Yamada, D. N. Futaba, S. Yasuda, O. Tanaike, H. Hatori, M. Yumura, S. Iijima, and K. Hata, "Compact and Light Supercapacitor Electrodes from a Surface-Only Solid by Opened Carbon Nanotubes with 2 200 m 2 g −1 Surface Area," *Adv. Funct. Mater.*, vol. 20, no. 3, pp. 422–428, Feb. 2010.

[20] C.-F. Sun, K. Karki, Z. Jia, H. Liao, Y. Zhang, T. Li, Y. Qi, J. Cumings, G. W. Rubloff, and Y. Wang, "A beaded-string silicon anode.," *ACS Nano*, vol. 7, no. 3, pp. 2717–24, Mar. 2013.

[21] N. Liu, Z. Lu, J. Zhao, M. T. McDowell, H.-W. Lee, W. Zhao, and Y. Cui, "A pomegranate-inspired nanoscale design for large-volume-change lithium battery anodes.," *Nat. Nanotechnol.*, vol. 9, no. 3, pp. 187–92, Mar. 2014.

[22] Z. Lu, N. Liu, H.-W. Lee, J. Zhao, W. Li, Y. Li, and Y. Cui, "Nonfilling carbon coating of porous silicon micrometer-sized particles for high-performance lithium battery anodes.," *ACS Nano*, vol. 9, no. 3, pp. 2540–7, Mar. 2015.

[23] N. Nitta and G. Yushin, "High-Capacity Anode Materials for Lithium-Ion Batteries: Choice of Elements and Structures for Active Particles," *Part. Part. Syst. Charact.*, vol. 31, no. 3, pp. 317–336, Mar. 2014.

[24] L.-F. Cui, Y. Yang, C.-M. Hsu, and Y. Cui, "Carbon-silicon core-shell nanowires as high capacity electrode for lithium ion batteries.," *Nano Lett.*, vol. 9, no. 9, pp. 3370–4, Sep. 2009.

[25] S.-H. Ng, J. Wang, D. Wexler, K. Konstantinov, Z.-P. Guo, and H.-K. Liu, "Highly reversible lithium storage in spheroidal carbon-coated silicon nanocomposites as anodes for lithium-ion batteries.," *Angew. Chem. Int. Ed. Engl.*, vol. 45, no. 41, pp. 6896–9, Oct. 2006.

[26] "Lithium hexafluorophosphate solution in ethylene carbonate and diethyl carbonate, 1.0 M LiPF6 in EC/DEC=50/50 (v/v), battery grade | Sigma-Aldrich." [Online]. Available: http://www.sigmaaldrich.com/catalog/product/aldrich/746746?lang=en&region=US. [Accessed: 03-Aug-2015].